Journal of Molecular Liquids 347 (2022) 118283

Contents lists available at ScienceDirect

Journal of Molecular Liquids

journal homepage: www.elsevier.com/locate/molliq

# Using all-atom simulations in explicit solvent to study aggregation of amphipathic peptides into amyloid-like fibrils

Sharareh Jalali [a], Yanxing Yang [a], Farbod Mahmoudinobar [a], Shaneen M. Singh [b], Bradley L. Nilsson [c], Cristiano Dias [a,*]

[a] Department of Physics, New Jersey Institute of Technology, Newark, NJ 07102-1982, United States
[b] Department of Biology, Brooklyn College, The City University of New York, Brooklyn, NY 11210, United States
[c] Department of Chemistry, University of Rochester, Rochester, NY 14627, United States

ARTICLE INFO

*Article history:*
Received 27 July 2021
Revised 7 November 2021
Accepted 4 December 2021
Available online 9 December 2021

*Keywords:*
Self-assembly
Amyloid
Molecular dynamics
Amphipathic peptides

ABSTRACT

Here, we perform all-atom molecular dynamics simulations in explicit solvent to study the aggregation of amphipathic peptides into amyloid-like fibrils. We use large simulation boxes containing more than 200,000 atoms and including 50 peptides to account for peptide concentrations of the order of 30 mM. Six different peptide sequences are studied in this work. We show that when long simulations (2–3 $\mu s$) are performed, a positive correlation is observed between experiments and simulations. In particular, peptide sequences that do not form fibrils in experiments show a low propensity to form inter-peptide hydrogen bonds and $\beta$-structures, and vice versa. Simulations are also performed at different temperatures and NaCl concentration to highlight the importance of hydrophobic and electrostatic interactions on aggregation. The rate of fibril formation in our simulations increases with increasing temperature for amphipathic peptides made from highly hydrophobic amino acids. This phenomena is related to the strength of hydrophobic interactions that enhances with increasing temperature. Electrostatic interactions may be responsible for the preference of anti-parallel $\beta$-sheets in our simulations. However, screening these interactions with NaCl favors aggregation of amphipathic peptides made from less hydrophobic amino acids. The sequence of events leading to fibril growth in our simulations is also discussed.



## 1. Introduction

The self-assembly process by which peptides organize themselves into one-dimensional structures is ubiquitous in nature. It is related to several neurodegenerative diseases including Alzheimer's and Parkinson's, and to functional biomaterials used by different organisms to gather food and/or for protection, e.g., silk in spiderwebs and silkmoth eggshells [1,2]. In recent years, considerable effort has been dedicated to fine-tune the properties of these materials to make them suitable for different biotechnological applications including drug delivery systems and tissue engineering [3–10]. These properties emerge from the supramolecular one-dimensional structure of the peptide assembly, which is characterized by the stacking of long $\beta$-sheets on top of each other accounting for the cross-$\beta$ signature of amyloid-like fibrils [11,12]. Currently, our understanding of the forces driving this self-assembly process and the critical events on pathway to fibril formation remains incomplete [13,14]. It requires probing peptide structures with atomic precision over micro- to millisecond timescales, which is beyond reach of most experimental methods but is becoming accessible to all-atom simulations in explicit solvent. This type of knowledge is expected to improve our understanding of amyloids in biological organisms as well as enable the development of better sequence-structure predictive tools.

Strictly amphipathic peptides are often used as a starting point in the design of new amyloid-like fibril structures [15,16]. Consecutive residues in these peptides alternate between non-polar (**X**) and polar (Y and Z) amino acids, i.e., $(\mathbf{XYXZ})_n$. Of particular interest to this work are neutral amphipathic peptides with $n = 2$ and where polar residues are positively and negatively charged lysine (Y = K) and glutamic acid (Z = E), respectively. Each of the two $\beta$-sheets that accounts for fibrils from these peptides have one of their faces decorated with non-polar side chains of **X** residues and the other face with charged K and E side chains–see Fig. 1. These $\beta$-sheets are anti-parallel in nature to provide the proper alignment for the interaction between positive K and negative E residues in neighboring strands [17]. In the fibril, side chains of

* Corresponding author.
*E-mail address:* cld@njit.edu (C. Dias).

https://doi.org/10.1016/j.molliq.2021.118283
0167-7322/

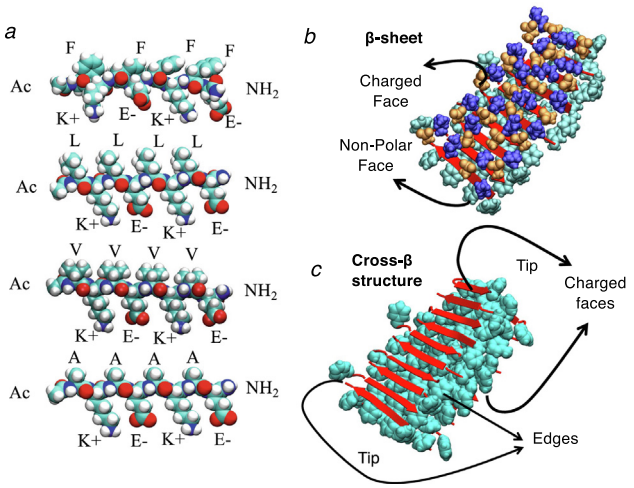


**Fig. 1.** Cross-$\beta$ structure of strictly amphipathic sequences Ac-(**X**K**X**E)$_2$-NH$_2$, where K and E represent positively and negatively charged lysine and glutamic acid, respectively. (a) Atomic structures of peptides in which the non-polar residue **X** is phenylalanine (F), leucine (L), valine (V), or alanine (A). (b) $\beta$-sheet from strictly amphipathic sequences wherein charged and non-polar residues are exposed to different faces of the sheet. Non-polar side chains are depicted in cyan. Purple and orange colors are used for lysine and glutamic acid, respectively. (c) Packing of two $\beta$-sheets into a cross-$\beta$ structure wherein the dry core is formed by non-polar side chains in cyan.

polar K and E residues are exposed to the solvent whereas non-polar faces of $\beta$-sheet are buried against each other forming a stable dry core–see Fig. 1. This type of cross-$\beta$ structure formed by strictly amphipathic sequences correspond to the symmetry class 5 in the Sawaya/Eisenberg classification scheme of fibrils [18,19].

One of the challenges of studying fibril formation is that the aggregation process is strongly sensitive to experimental conditions. Thus, it is important to compare experiments performed under the same conditions when studying the effect of the peptide sequence. Experimental studies have explored the role of hydrophobicity in fibril formation by probing different non-polar amino acids at position **X** of the (**X**K**X**E)$_2$ sequence [20,21]. For the least hydrophobic amino acid, i.e., alanine (X = A), peptides did not self-assemble up to a concentration of 8 mM [22,20]. In contrast, peptides made from the more hydrophobic amino acids, i.e., phenylalanine (F), leucine (L) or valine (V), formed amyloid fibrils already at concentrations of 0.2 mM [22,20]. The net hydrophobicity is, however, not the only factor accounting of a sequence's propensity to form fibrils as amphipathic sequences in which pairs of non-polar residues are flanked by charged residues, i.e., (K**FF**E)$_2$, did not form fibrils at concentrations up to 1 mM as opposed to KE**FFFF**KE or the strictly amphipathic (**FK**F**E**)$_2$ sequence [17]. This profound influence of the sequence pattern on fibril formation was related to its effect on the propensity of a peptide to form $\beta$-sheets and its ability to enable non-polar and charged side chains to segregate to different faces of a $\beta$-sheet [17].

Insights into general principles of fibril formation are often studied using coarse grained models [23]. For example, peptide sequences exhibiting low and high $\beta$-strand propensities have been shown to favor the formation of disordered aggregates and amyloid fibrils, respectively, whereas on-pathway intermediates emerge only for peptides with a medium propensity to form $\beta$-strands [24,25]. More recently, the phase diagram of a fragment of the A$\beta_{16-22}$ peptide was studied as a function of temperature using the coarse grained PRIME20 force field wherein the solubility line predicted by these simulations provided some agreement with experiments [26]. Many of the coarse grained model predictions were made prior to experiments, which highlights the importance of these models in providing new insights and guiding experiments [23]. However, the use of simplified models has also its limitations including that they cannot provide atomic level insights that are needed for drug discovery, for a detailed and reliable description of the mechanisms of aggregation, or to understand fibril polymorphism.

All-atom simulations in explicit solvent have the potential to provide a more complete picture of the aggregation process by characterizing the sequence of events and the molecular mechanisms accounting for fibril formation [14,27]. However, simulations starting with peptides randomly distributed in space which aggregate into amyloid fibrils are very time consuming as they require tracking a large number atoms (e.g., $> 200,000$ atoms to account for peptide concentrations of the order of 10 mM) for a long time ($> 1\mu s$). Moreover, it is not possible to fully reproduce experimental conditions [13] and the ability of force fields to account for fibril formation remains a question of debate [28,29]. Accordingly, simulations of spontaneous aggregation using all-atom models have been performed for only a small number ($< 10$) of short peptides, which mostly do not self-assemble into stable cross-$\beta$ structures. A case in point is the A$\beta_{16-22}$ peptide for which only a limited number of force fields can account for its aggregation within 1 $\mu s$ [28]. The promising results obtained for this peptide using the CHARMM36m force field suggest that, at least for short peptide sequences, all-atom simulations will soon reach a state where they can work hand-in-hand with experiments complementing each other [28]. Regarding the amphipathic (K**FF**E)$_1$ sequence, recent all-atom simulations of tetramers have illustrated the challenge of interconverting disordered aggregates into ordered ones [30]. Short femtosecond-long all-atom simulations of (**FK**F**E**)$_2$ peptides have also been performed to test the stability of different fibril structures varying in the hydrogen bond pattern of their $\beta$-sheets [31,32].

Here, we expand on these computational studies by performing large-scale (50 peptides in a simulation box containing more than ~200,000 atoms) and long-time simulations to provide insights into the aggregation process of six peptide sequences at different conditions of temperature and salt-concentration. Some of our simulations are more than one order of magnitude (10–14 $\mu s$) longer than the length of most all-atom molecular dynamics studies of aggregation (0.5–1 $\mu s$). We show that, in most cases, the latter timescale is not enough to enable the formation of cross-$\beta$ structures or to discriminate the aggregation process of different amphipathic peptide sequences. However, when longer ($>$ 2–3 $\mu s$) simulations are performed, we observe a positive correlation between aggregation *in silico* and *in vitro* wherein sequences that do not form fibrils in experiments have a low propensity to form inter-peptide hydrogen bond and $\beta$ -structures in our simulations. Moreover, we show that increasing temperature causes aggregation to take place faster for highly hydrophobic amino acids, which we relate to the enhanced strength of hydrophobic interactions with increasing temperature. A preference for the formation of anti-parallel $\beta$ -sheets is also observed in fibrils that formed spontaneously in our simulations. Whereas electrostatic interactions are expected to drive this preference, these interactions may also be unfavorable to fibril formation [33]. In our simulations, screening these interactions by adding salt to the solution increased the preference for fibril formation.

## 2. Methodology

**System Design, Equilibration and Simulation.** Four strictly amphipathic peptides with sequences alternating between non-polar (represented by the letter **X**) and charged (represented by

letters **E** and **K** for the negatively and positively charged glutamic acid and lysine residues, respectively) residues were investigated in this study. These eight-residue peptides were capped with an acetyl group (Ac) at the N terminus and an amide group ($NH_2$) at the C terminus, i.e., Ac-(**X**K**X**E)$_2$-$NH_2$. The four peptides studied here differ in the degree of hydrophobicity of their non-polar residue, which is either phenylalanine (F), leucine (L), valine (V), or alanine (A)–see Fig. 1. We will refer to these strictly amphipathic sequences as F-, L-, V-, and A-peptides. Experimentally, the more hydrophobic F-, L-, and V-peptides were shown to form fibrils as opposed to the less hydrophobic **A**-peptide [20]. We also performed simulations of two sequences that are amphipathic but they do not have alternating hydrophilic/hydrophobic sequence order, i.e., Ac-(KE**FFFF**KE)-$NH_2$ and Ac-(K**FF**E)$_2$-$NH_2$. Self-assembly into amyloid fibrils was observed in experiments using the former peptide sequence at concentrations of 1 mM but not the latter [17].

Simulations in this work were prepared in two steps. First, 50 peptides were randomly place in a cubic box of length 8 nm, which was then solvated and the energy of the system minimized followed by a 4 ns equilibration in the NVT ensemble. Second, to avoid creating a self-assembly process in which an elongated aggregate interacts with itself through periodic boundary conditions, the size of the simulation box was increased to 13.5 nm and solvated accounting for a peptide concentration of 37 mM. The energy of the system was minimized and equilibrated in the NVT ensemble.

**Software, Hardware, and parameters.** MD simulations were performed with the Amber99sb-ILDN force field [34] and the TIP3P water model by applying periodic boundary conditions in the isothermal-isobaric (NPT) ensemble. The leapfrog algorithm was used to integrate the equations of motion with a 2 fs time-step [35]. The Parrinello-Rahman barostat ($\tau_p = 2.0$ ps) was used to maintain the pressure of the system at 1 bar [36]. Temperature was controlled by coupling protein and solvent separately to the velocity-rescale thermostat ($\tau_t = 0.1$ ps). The cut-off for short range van der Waals and electrostatic interactions was 1.0 nm. The smooth Particle Mesh Ewald algorithm was used to compute long range electrostatic interactions [37]. For all systems, the production run started with a 100 ns simulation in the NPT ensemble using GROMACS [38]. Some of these simulations were then extended either on Anton 2 supercomputer [39] or on our local cluster using GROMACS–see table S1 for a list of all simulations performed here [40].

**Analysis**. To quantify the extent of by which peptides self-assemble into $\beta$-sheets in our simulations, we track the number of hydrogen bonds ($N_{HB}$) between backbone atoms over time [41]. This quantity is also decomposed into contributions from intra- (intra-$N_{HB}$) and inter-backbone (inter-$N_{HB}$) hydrogen bonding. We consider that an hydrogen bond forms when the distance between donor and acceptor atoms is less than or equal to 0.35 nm and the angle between hydrogen, donor and acceptor atoms is less than or equal to 30 degree. Contact maps (CM) were used to provide insights into inter-peptide interactions formed during the self-assembly process. For that purpose, two residues are considered to be in contact if the distance between any pair of their respective atoms is less than or equal to 0.4 nm. The sum of inter-peptide contacts was normalized to account for a probability of contacts. The python scripts provided by the Strodel group [42] were used for that purpose with the required libraries [43–45]. Secondary structures were defined using the DSSP (*Define Secondary Structure of Proteins*) algorithm [46].

## 3. Results and Discussions

### 3.1. Role of hydrophobic interactions on fibril formation

In Fig. 2, we show the time dependence of the total number of backbone hydrogen bonds, i.e., $N_{HB}$, for simulations performed using strictly amphipathic sequences in pure water. A logarithmic scale is used for the x-axis to highlight the aggregation process at short timescales when $N_{HB}$ is subjected to large changes. Panel a shows that, for the F-peptide at 350 K (black line), $N_{HB}$ increases with time and it starts saturating after approximately 4 $\mu$s. This saturation is better appreciated using a linear scale for the x-axis, which is provided in Fig. S4 [40]. At 300 K (green line), $N_{HB}$

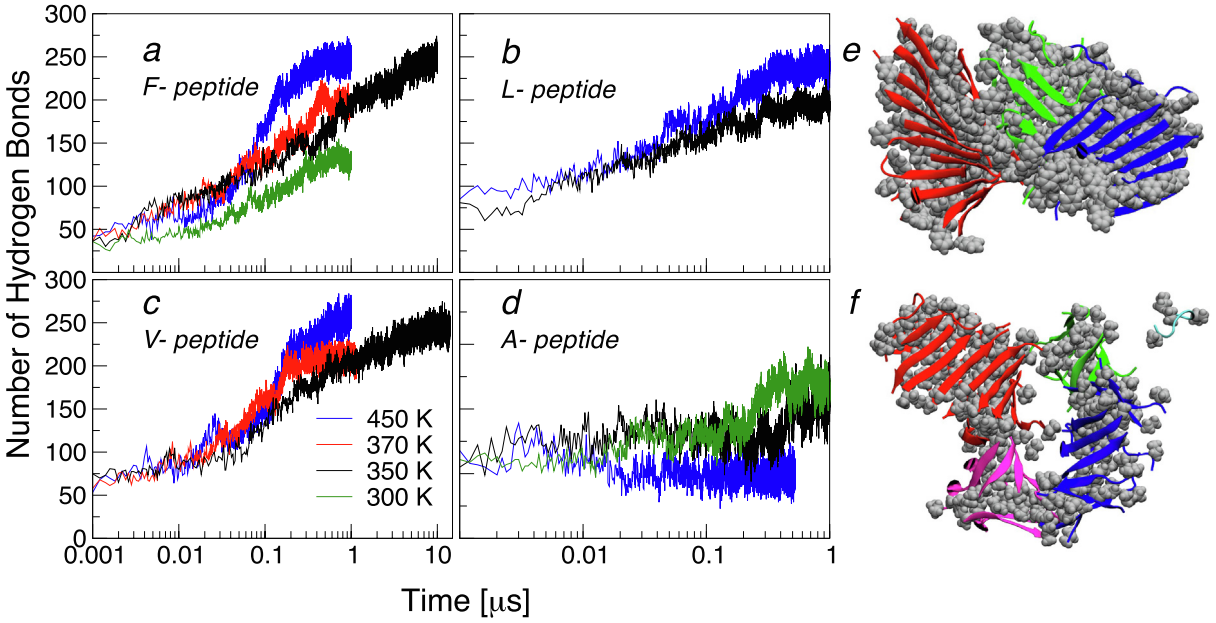


**Fig. 2.** Effect of temperature on self-assembly. Backbone hydrogen bond formation in our simulations using strictly amphipathic (a) F-, (b) L-, (c) V-, and (d) A-peptides at different temperatures. Last configuration in our simulations performed at 350 K using (e) F- and (f) V-peptides. van der Waals representation is used to depict non-polar side chains in gray and secondary-structures are shown using a cartoon representation where $\beta$-sheets are shown by arrows. Different colors are used for cross-$\beta$ structures that are not (or are loosely) connected to each other via hydrogen bonds.

increases at a significantly slower pace than at 350 K suggesting that increasing temperature accelerates the self-assembly process that leads to fibril formation. Note that recent experimental studies have reported a similar effect for elastin-based peptides over the temperature range 293–353 K [47]. To further highlight this effect of temperature, we perform additional simulations at extreme temperatures of 370 and 450 K. Simulations at these extreme temperatures should, however, be taken with caution and they are only used here to highlight the trend observed at 300 and 350 K. The increase in $N_{HB}$ at 370 K occurs at approximately the same rate as in our simulations at 350 K but it takes place significantly faster at 450 K saturating after only 0.6 $\mu$s. Temperature has a similar effect on $N_{HB}$ for the L- and V-peptides in panels b and c. In particular, for the L-peptide, $N_{HB}$ increases significantly faster at 450 K than at 350 K. For the V-peptide at 450 K, $N_{HB}$ saturates after only 0.6 $\mu$s whereas 10 $\mu$s are required for this to happen at 350 K. For the less hydrophobic A-peptide, $N_{HB}$ does not increase in a significant manner at any temperature–see panel d. This is consistent with experimental studies highlighting the importance of hydrophobic interaction in the formation of stable aggregations [20,22]. Moreover, at any time during the simulation, this less hydrophobic peptide forms less hydrogen bonds at the higher temperature (450 K) than at lower temperatures, i.e., 300 K and 350 K.

At first sight the faster aggregation of F-, L-, and V-peptides with increasing temperature is counterintuitive as temperature favors states with higher entropy wherein peptides would be dispersed in the simulation box. However, hydrophobic interactions play an important role in the attraction between amphiphilic peptides and the strength of these interactions increases with increasing temperature to maximize the entropy of the solvent [48–52]. Hydrophobicity is therefore expected to be the force driving peptide self-assembly in our simulations of F-, L-, and V- peptides, as it can explain the increased rate of aggregation with increasing temperature in panels a-c. This is consistent with studies showing that amyloid fibrils that have a non-polar core become more stable with increasing temperature [53,47,54–56]. In the same vein, the inability of the A-peptide to self-assemble and form fibrils in simulations (see panel d) and experiments [20,22] can be explained by the reduced hydrophobic nature of this peptide.

Final structures of simulations performed using F- and V-peptides at 350 K are shown in Fig. 2 e-f. In these structures, peptides form cross-$\beta$ structures with most non-polar side chains (in gray) buried away from the solvent. A different color is used to represent cross-$\beta$ structures that are not connected to each other through backbone hydrogen bonds highlighting different unit blocks. Notice that solvent exposed non-polar side chains are located either at the tip or at the edge of cross-$\beta$ structures. Burial of these exposed non-polar side chains away from the solvent drives packing of cross-$\beta$ units in our simulations. Because phenylalanine has a bulkier side chain than valine, edges of cross-$\beta$ structures from F-peptides have more exposed non-polar surface area than for V-peptides–see Fig. 2e-f. Accordingly, non-polar side chains at edges and tip of cross-$\beta$ structures in our simulations of the F-peptide are buried against each other–see blue and green as well as red and green cross-$\beta$ structures in Fig. 2e. For the V-peptide, the different cross-$\beta$ structures are connected to each other mostly through the "tip" which has exposed non-polar side chains. Last configurations of L- and A-peptides in our simulations at 350 K and 450 K are shown in Fig.S2 [40].

To further highlight the importance of non-polar burial, we show in Fig. 3 the time dependence of both the solvent accessible surface area (i.e., SASA) of non-polar side chains and $N_{HB}$. For F-, L-, and V-peptides, SASA (black lines) and $N_{HB}$ (blue lines) decreases and increases, respectively, with time as hydrophobic interactions between non-polar side chains and hydrogen bonds between backbone atoms form during fibrilization. This shows strong correlation between non-polar burial and $\beta$-sheet formation. For the A-peptide (panel e), SASA and $N_{HB}$ change only modestly due to the lack of cross-$\beta$ structure formation. Contact maps (i.e., CM) computed during the last 500 ns in our simulations at 350 K are shown in Fig. 4 to depict pairs of residues involved in interpeptide interactions. Contacts between non-polar residues for F-, L-, and V-peptides occur at least twice more frequently than between charged K and E residues. These non-polar contacts are formed with neighboring residues on the same $\beta$-sheet as well as with residues on the other sheet of the cross-$\beta$ structure. Conversely, charged residues, which are facing the solvent, can only form contacts with neighboring residues on the same $\beta$-sheet. Notice that because of the absence of a dry core for the A-peptide, both non-polar and charged residues interact with approximately the same probability in our simulations. Fig. 4 also depicts a tendency of peptides to form antiparallel contacts wherein the first residue interacts preferentially with the last or second to last non-polar residue. Accordingly, 72% and 65% of all pairs of neighboring strands for F- and V- peptides in Figs. 2e-f form anti-parallel $\beta$-sheets. Electrostatic interactions between charged side chains can be used to discriminate

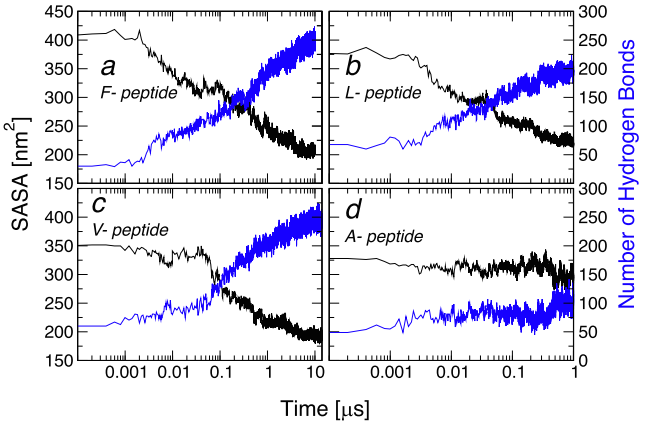


**Fig. 3.** Burial of non-polar side chains. The time-dependence of the solvent accessible surface area (SASA) of non-polar residues is shown for (a) F-, (b) L-, (c) V-, and (d) A-peptides from simulations performed at 350 K. The number of backbone hydrogen bonds is also shown in blue.

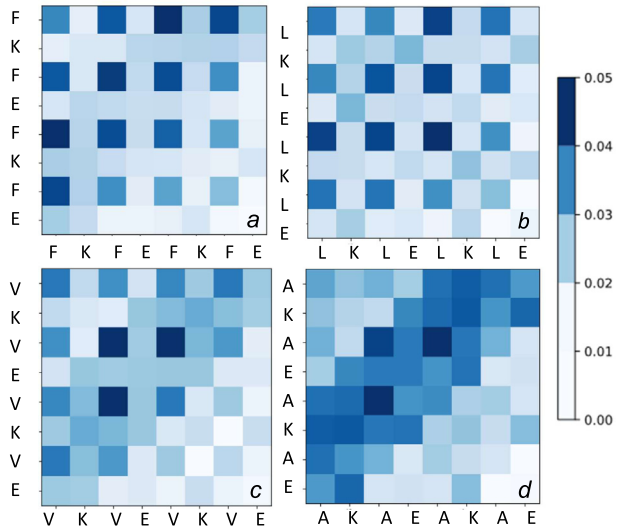


**Fig. 4.** Contact maps computed for strictly amphipathic (a) F-, (b) L-, (c) V-, and (d) A-peptides in simulations performed at 350 K. Only the last 500 ns of our simulations are used in the calculation of contact maps.

parallel and anti-parallel $\beta$-sheets[20]. In a parallel setup, like-charged residues (K–K or E–E) of neighboring strands face each other whereas, in anti-parallel $\beta$-sheets, opposite-charged pairs of residues (K–E) of neighboring strands face each other optimizing electrostatic interactions.

### 3.2. Growth of cross-$\beta$ structures

Fig. 5 depicts the time evolution of secondary structures in our simulations. Initially, peptides are mostly disordered and, thus, residues adopt preferentially coil (see panel b) or bend/turn (see panel c) conformations. As the simulation evolve in time, the fraction of residues adopting $\beta$ conformations increases from 0.1 to 0.5 for F- and V- peptides and from 0.1 to 0.3 for L-peptides. Congruently, the number of disordered residues (coil and bend/turn in panels b and c) decreases proportionally. For the A-peptide, the fraction of residues adopting $\beta$ conformations increases only marginally from 0.1 to 0.2. Similarly the number of disordered residues for the A-peptide, i.e., coil and bend/turn conformations, do not decrease significantly as in the case of the more hydrophobic sequences. This is consistent with this peptide not forming fibrils in the 1 $\mu$s time-frame in our simulations. The fraction of residues in helical conformations is not significant for the more hydrophobic peptides and it is small (but not zero) for the A-peptides consistent with the high propensity of alanine to form $\alpha$-helices [57].

To provide insights into the formation of cross-$\beta$ structures in our simulations, we identified the peptides that are part of the different $\beta$-sheets at the end of our simulations and computed separately the number of backbone hydrogen bonds between these peptides as a function of time. For the F-peptide, seven $\beta$-sheets varying in size from two (black color in Fig. 6a) a) to eleven (red color) peptides are present at the end of our 350 K simulation.

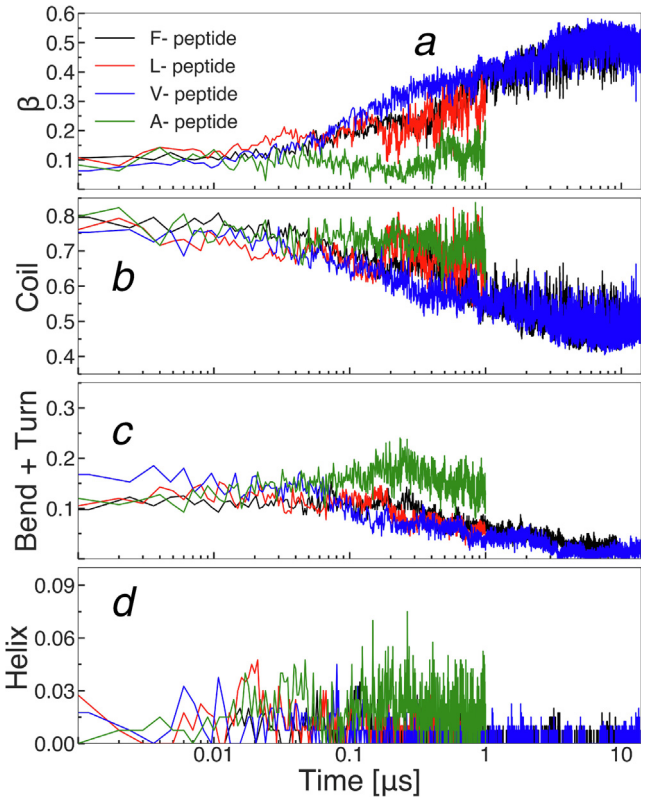


**Fig. 5.** Secondary structures of strictly amphipathic peptides in simulations performed at 350 K. Fraction of all residues adopting (a) $\beta$, (b) coil, (c) bend + turn, and (d) helical conformations as a function time.

The two $\beta$-sheets with the highest number of hydrogen bonds (red and blue lines) at the end of the simulation are part of the same cross-$\beta$ structure. Similarly, sheets with the third and fourth highest number of hydrogen bonds (light blue and purple) are part of the same cross-$\beta$ structure. The smallest cross-$\beta$ structure in our simulation is made from the $\beta$-sheets with fifth and sixth highest number of hydrogen bonds (yellow and green lines in Fig. 6). This suggests a correlation between the growth of the two sheets that are part of the same cross-$\beta$ structures.

Fig. 6b-g illustrates the growth of the largest cross-$\beta$ structure represented by red and blue $\beta$-sheets in panel a. At 0.7 $\mu$s (panel b), a $\beta$-sheet extending over seven peptides (in blue) has already formed on top of which two small $\beta$-sheets (in red) are deposited at the extremity of its non-polar face. Non-polar side chains of these "blue" and "red" sheets are packed against each other forming stable dry cores. Growth of both red and blue $\beta$-sheets occur concurrently via displacement of peptides located in their vicinity towards the tip–see arrows in panel b-g. Also, peptides are being deposited in the space between the two red sheets. This is illustrated in panels d-g where yellow and light red peptides land in between the two red $\beta$-sheets forming hydrogen bonds with both of them. Initially, the yellow peptide is folded into a $\beta$-hairpin–panel e. Unfolding of the $\beta$-hairpin enables this yellow peptide to become extended where it forms hydrogen bonds with just one of the red sheets without interacting with the other red sheet–see panel f. Displacement of red sheets along the main axis of the cross-$\beta$ structure allows the yellow peptide to connect the two red sheets via hydrogen bonds–see panel g. This depicts the formation of a cross-$\beta$ structure wherein one sheet behaves as the substrate on top of which peptides are being deposited.

In Fig. 7, we show the growth of different $\beta$-sheets in simulations performed using the V-peptide at 350 K. At the end of the simulation, we identify eight sheets that are not (or are only loosely) connected to each other via backbone hydrogen bonds. The two largest sheets (represented in red and blue) in panel a are part of the same cross-$\beta$ structure. At 2.1 $\mu$s (panel b), each of these sheets contain four peptides. As for the F-peptide, the growth of these sheets occurs mainly via the displacement of peptides that are located in their vicinity towards the tip–see arrows in panels b-e. In addition to this cross-$\beta$ structure, six $\beta$-sheets that are only loosely connected to each other through hydrogen bonds are present at the end of our simulation. These sheets are highly distorted enabling the formation of a dry core within themselves where valine side chains are buried away from water. The evolution of two of those $\beta$-sheets is depicted in light blue and brown colors in panels b-g. They correspond to sheets with the third and fourth largest $N_{HB}$ in panel a. These sheets form early and they remain stable throughout the simulation. The absence of distorted $\beta$-sheets in our simulations using the F-peptide may be explained by the bulky side chain of phenylalanine, which imposes steric constrains on compact conformations.

### 3.3. Role of the amino acid sequence pattern on fibril formation

The net hydrophobicity of amphipathic sequences is an important factor determining the ability of peptides to form amyloid-like fibrils. However, experimental studies have also highlighted the importance of the sequence pattern on the self-assembly process [58,15,59]. In particular, peptides composed of identical amino acids as the F-peptides but with non-polar and charged residues located at different positions in the sequence have been tested for fibril formation [17]. Two such peptides are amphipathic Ac-(K**FF**E)$_2$-$NH_2$ and Ac-KE**FFFF**KE-$NH_2$ sequences that have non-polar segments made from two and four consecutive phenylalanines, respectively, flanked by charged residues. Compared to the F-peptide, which forms fibrils at concentrations of 0.2 mM and 1 mM,

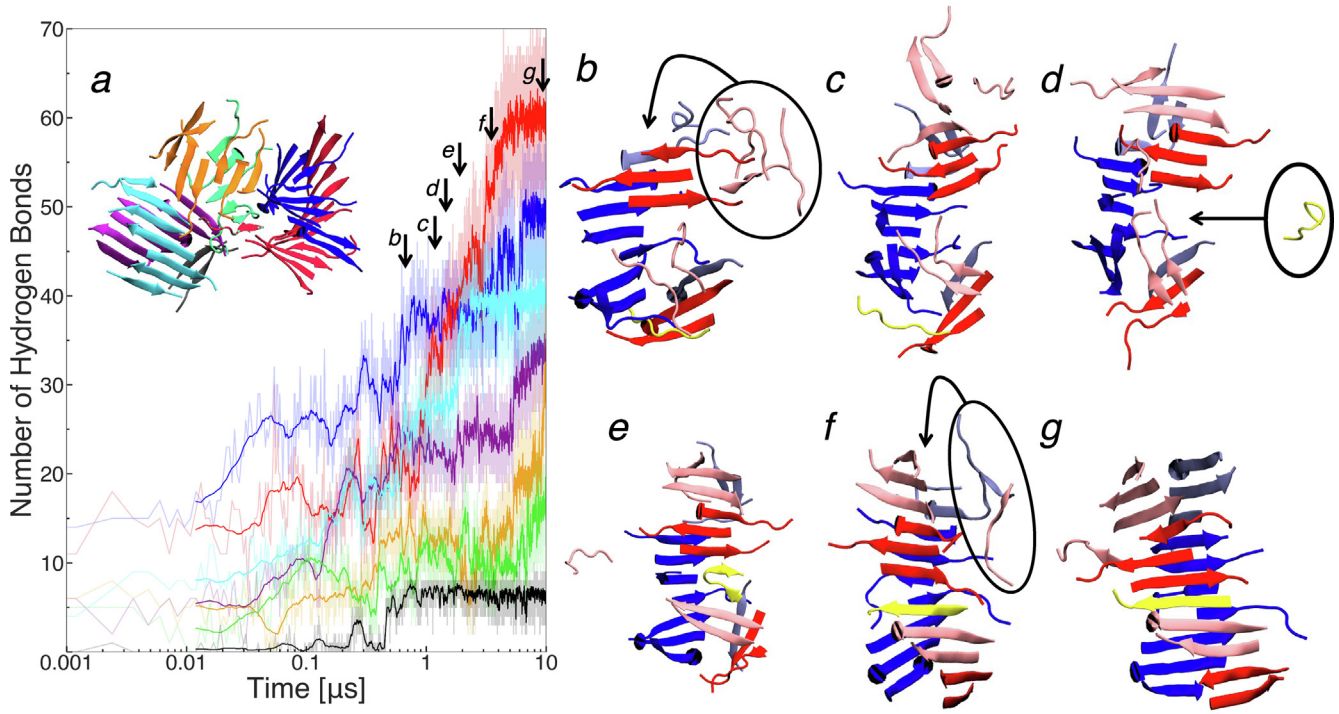


**Fig. 6.** Growth of the seven $\beta$-sheets that formed spontaneously in our simulation performed using F-peptides at 350 K. a) Number of backbone hydrogen bonds of each $\beta$-sheet as a function of time. Thick lines are a guide to the eye and they correspond to moving averages over 25 ns. Panels b, c, d, e, f, and g correspond to the configurations of two sheets at time 0.7 $\mu$s, 1.1 $\mu$s, 1.5 $\mu$s, 1.9 $\mu$s, 3.5 $\mu$s and 10 $\mu$s, respectively. Disordered monomers in the vicinity of the sheets are drawn in light red and light blue.

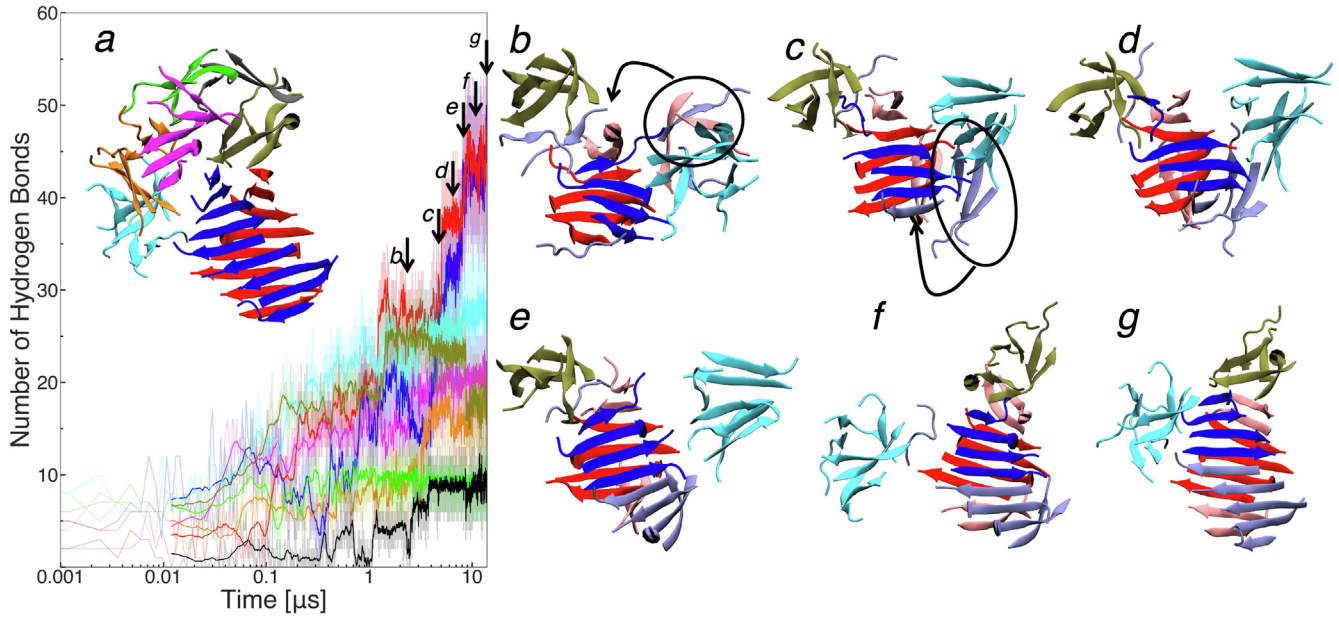


**Fig. 7.** Growth of the eight $\beta$-sheets that formed spontaneously in our simulation performed using V-peptides at 350 K. a) Number of backbone hydrogen bonds of each $\beta$-sheet as a function of time. Thick lines are a guide to the eye and they correspond to moving averages over 25 ns. Panels b, c, d, e, f, and g correspond to the configurations of two sheets at time 2.1 $\mu$s, 5.6 $\mu$s, 6.4 $\mu$s, 8.1 $\mu$s, 11.5 $\mu$s and 14 $\mu$s, respectively. Disordered monomers in the vicinity of the sheets are drawn in light red and light blue.

Ac-KE**FFFF**KE-$NH_2$ only formed fibril at 1 mM, and Ac-(K**FF**E)$_2$-$NH_2$ does not self-assemble at both concentration [17]. A possible explanation for this sequence pattern effect may come from the low propensity of K and E residues to form $\beta$-sheets [57]. The less fibril-prone sequences have patches with two consecutive charged residues, i.e., EK or KE, which may reduce the propensity of peptides to form $\beta$-strands specially when located in the middle of the sequence–as in the case of the Ac-(K**FF**E)$_2$-$NH_2$ peptide [17]. Also, the inability of non-polar and charged residues to be segregated into different faces of a $\beta$-sheet for Ac-(K**FF**E)$_2$-$NH_2$ and Ac-KE**FFFF**KE-$NH_2$ peptides is expected to contribute to their reduced propensity to form fibrils [17].

To provide insights into effects of sequence pattern on the self-assembly process of the F-peptide, we performed additional 4 $\mu$s simulations using Ac-(K**FF**E)$_2$-$NH_2$ and Ac-KE**FFFF**KE-$NH_2$ peptides. All simulations were performed under the same conditions

described in the methodology section for the F-peptide. Fig. 8a compares the evolution of the total number $N_{HB}$ of backbone hydrogen bonds for these peptides over time. The F-peptide forms hydrogen bonds much faster than the other two peptides, consistent with its higher experimental propensity to form fibrils. Moreover, after 4 $\mu$s most F-peptides in our simulations adopt $\beta$-sheet structures–see Fig. 8d. The time evolution of $N_{HB}$ is very similar for Ac-KE**FFFF**KE-$NH_2$ and Ac-(K**FF**E)$_2$-$NH_2$ sequences although their final structures are significantly different–see Fig. 8e-f. A cross-$\beta$ structure and several large $\beta$-sheets comprising 4–5 peptides are observed in simulations using Ac-KE**FFFF**KE-$NH_2$ peptides (panel c) while Ac-(K**FF**E)$_2$-$NH_2$ peptides (panel d) adopt mostly coil and turn structures with high propensity. These structural differences are in line with experiments showing that the Ac-KE**FFFF**KE-$NH_2$ sequence has a greater probability of forming fibrils compare to Ac-(K**FF**E)$_2$-$NH_2$.

The similarity in the time dependence of $N_{HB}$ for Ac-KE**FFFF**KE-$NH_2$ and Ac-(K**FF**E)$_2$-$NH_2$ sequences can be understood by decomposing this quantity into intra- and inter- peptide backbone hydrogen bonding, i.e., intra-$N_{HB}$ and inter-$N_{HB}$, respectively. These quantities are shown in Fig. 8b-c. The F-peptide (black line) forms less intra-$N_{HB}$ than the other two sequences and after 0.3 $\mu$s this quantity decreases continuously in the simulation (see panel b) while inter-$N_{HB}$ increases over time (see panel c). This characterizes the F-sequence as having a high propensity to interact with neighboring peptides via backbone hydrogen bonds. Although the initial intra-$N_{HB}$ for the Ac-KE**FFFF**KE-$NH_2$ sequence (red line) is much larger than for the F-peptide, this quantity also decreases after 0.3 $\mu$s (panel b) while inter-$N_{HB}$ increases continuously but modestly throughout the simulation (see panel c). Thus, this peptide also has a preference for interacting with neighboring peptides via backbone hydrogen bonds although this preference is smaller than for the F-peptide. The initial intra-$N_{HB}$ for the Ac-(K**FF**E)$_2$-$NH_2$ sequence (green lines) is comparable to the one for the Ac-KE**FFFF**KE-$NH_2$ peptide but this quantity does not decrease significantly during the simulation (panel b) and inter-$N_{HB}$ remained constant during the last 2 $\mu$s of our simulations (see panel c). This highlights the lack of propensity of the Ac-KE**FFFF**KE-$NH_2$ sequence to interact with neighboring peptides and aggregate.

In Fig. 8g-j, g-j, we show the time evolution of the fraction of residues in different secondary structures for F-, Ac-(K**FF**E)$_2$-$NH_2$ and Ac-KE**FFFF**KE-$NH_2$ sequences. These peptides are highly disordered in the beginning of the simulations with the fraction of all residues adopting coil and bend + turn structures being 0.7–0.9 and 0.1–0.2, respectively–see panel h-i. As the simulation progresses, peptides become more ordered and at 4 $\mu$s the fraction of residues in $\beta$-conformations is 0.48, 0.40, and 0.22 for F-, Ac-KE**FFFF**KE-$NH_2$, and Ac-(K**FF**E)$_2$-$NH_2$ peptides, respectively. This corroborates the order of decreasing fibril propensity for these sequences as measured experimentally. Interestingly, a residual number of $\alpha$-helices is observed in the reversed order of fibril propensity, i.e., Ac-(K**FF**E)$_2$-$NH_2$ > Ac-KE**FFFF**KE-$NH_2$ $\gg$F-peptide. Thus, sequences that do not form fibril in our simulations exhibit a non-negligible propensity to adopt helical structures. This includes the A-peptide (see Fig. 5) and Ac-(K**FF**E)$_2$-$NH_2$.

Fig. 9a-c shows contact maps of the three peptides studied here computed during the time-frame 2.5–3 $\mu$s. For all sequences, interactions are formed with higher probability between pairs of non-polar residues accounting for the dark pattern color in panels a-c. Contacts between charged amino acids occur with a significantly lower probability, which is consistent with the reported low propensity of K and E amino acids for $\beta$-structures [57]. In the case of the Ac-(K**FF**E)$_2$-$NH_2$ peptide, charged residues in the middle of the sequence make it difficult for $\beta$-structures to extend all the way from the N- to the C-terminus. Accordingly, we observe several short $\beta$-strands made of only two residues in Fig. 8f. The solvent accessible surface area (SASA) of non-polar residues for the three-peptides studied here is shown in Fig. 9d. This quantity decreases continuously for F- and Ac-KE**FFFF**KE-$NH_2$ sequences as non-polar side chains are buried away from the solvent during the formation of cross-$\beta$ structures. For the Ac-(K**FF**E)$_2$-$NH_2$ sequence, SASA decreases during the first 0.4 $\mu$s and then it increases during the remaining of the simulation. Combined with results from Fig. 8, this shows that the Ac-(K**FF**E)$_2$-$NH_2$ sequence

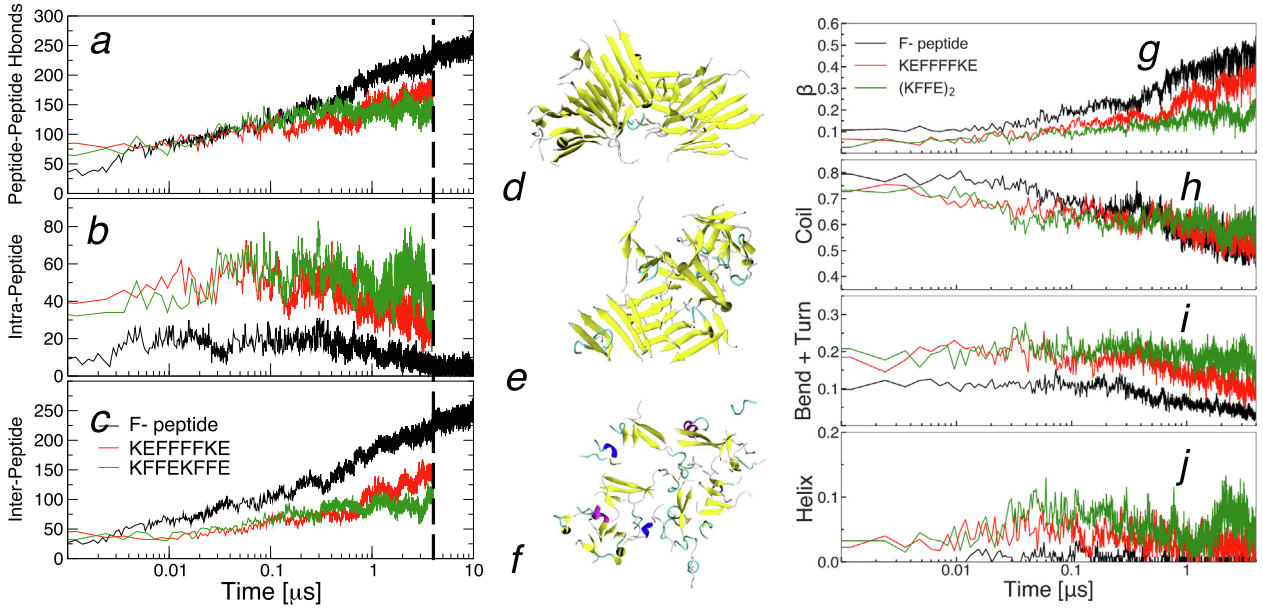


**Fig. 8.** Effect of sequence pattern on fibril formation. Time evolution of the number of (a) total, (b) intra-, and (c) inter-peptide backbone hydrogen bonds for F- (black), Ac-KE**FFFF**KE-$NH_2$ (red), and Ac-(K**FF**E)$_2$-$NH_2$ (green) peptides. Peptide configurations at 4 $\mu$s from simulations of (d) F-, (e) Ac-KE**FFFF**KE-$NH_2$, and (f) Ac-(K**FF**E)$_2$$NH_2$ peptides. Yellow, cyan, white, purple and blue colors are used to represent $\beta$-structures, turn, coil, $\alpha$-helix and 3–10 helix structures. Fraction of all residues adopting (g) $\beta$, (h) coil, (i) bend + turn, and (j) helical structures.

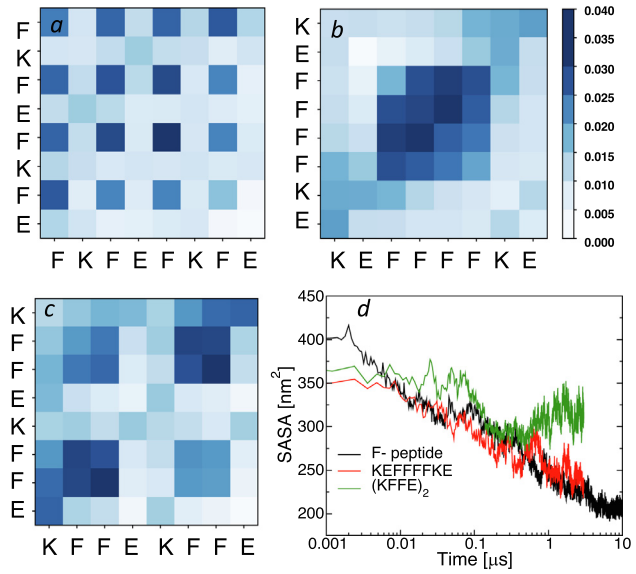


**Fig. 9.** Effect of sequence pattern on contact map and SASA. Contact maps computed within 2.5–3 $\mu s$ in our simulations using (a) F-peptide, (b) KE**FFFF**KE, and (c) (K**FF**E)$_2$. (d) Solvent accessible surface area of non-polar residues (SASA) for simulations performed using F-peptide (black), KE**FFFF**KE (red), and (K**FF**E)$_2$ (green).

does not form cross-$\beta$ structure as the number of inter-peptide hydrogen bonds and $\beta$-structures is not maximized in the simulation, and SASA is not minimized.

### 3.4. Role of electrostatic interactions on fibril formation

To provide additional insights into the lack of aggregation of the A-peptide, we show in Fig. 10 contact maps computed over the first (panel a) and the last (panel b) 500 ns in simulations performed at 350 K. These maps show a strong preference for contacts between charged residues in the beginning of the simulation (panel a) and a strong preference for non-polar contacts at the end of the simulation (panel b). Since, for the more hydrophobic peptides non-polar contacts dominate both the beginning (see S3 [40]) and the end of our simulations (see Fig. 4), this made us wonder if screening electrostatic interactions for the A-peptide would favor aggregation. To test this hypothesis, additional simulations of the A-peptide were performed in the presence of NaCl at concentrations of 40 mM. In panels c and d, we shown the time evolution of the number of inter-peptide hydrogen bonds (i.e., inter-$N_{HB}$) for two simulations performed in pure water and in the presence of 40 mM, respectively. Although results from these simulations are subjected to large fluctuations, the number of inter-peptide hydrogen bonds is larger in the presence of 40 mM NaCl than in pure water. This number averaged over the last 200 ns is 82 in pure water and 105 in the presence of NaCl. Final structures obtained from our simulations in the absence and presence of NaCl for one of the samples (black lines in Fig. 11c,d) are shown in panels g-h. Most of the peptides are dispersed in the pure water solution (panel g) and a much larger oligomer has formed in the presence of 40 mM (panel h). The latter consist mainly of $\beta$-sheets wherein one face is mostly populated with alanine side chains and the other with charged side chains. These results point to small preference for aggregation in presence of NaCl.

In an attempt to amplify the effect of NaCl and provide a more definite answer to the role played by electrostatic interactions, simulations were also performed at 80 mM and 160 mM. The number of inter-peptide hydrogen bonds and the SASA computed for non-polar residues are shown in panels e-f. Even at high concentrations, these quantities are subjected to large fluctuations. However, they highlight the same trend as observed for 40 mM in which the addition of NaCl to the solution accounts for a modest increase in inter-$N_{HB}$ compared to simulations performed in pure water. Also, the SASA computed in the presence of NaCl at any concentration is lower than the one computed in pure water, which is consistent with an increase in the propensity of peptides to aggregate. This propensity does not, however, increase monotonically with increasing NaCl concentration as effects of NaCl on aggregation are less pronounced at 160 mM NaCl than at 40 or 80 mM. Nevertheless, at all non-zero NaCl concentrations, inter-$N_{HB}$ and SASA are higher and lower, respectively, compared to simulations performed in pure water solution.

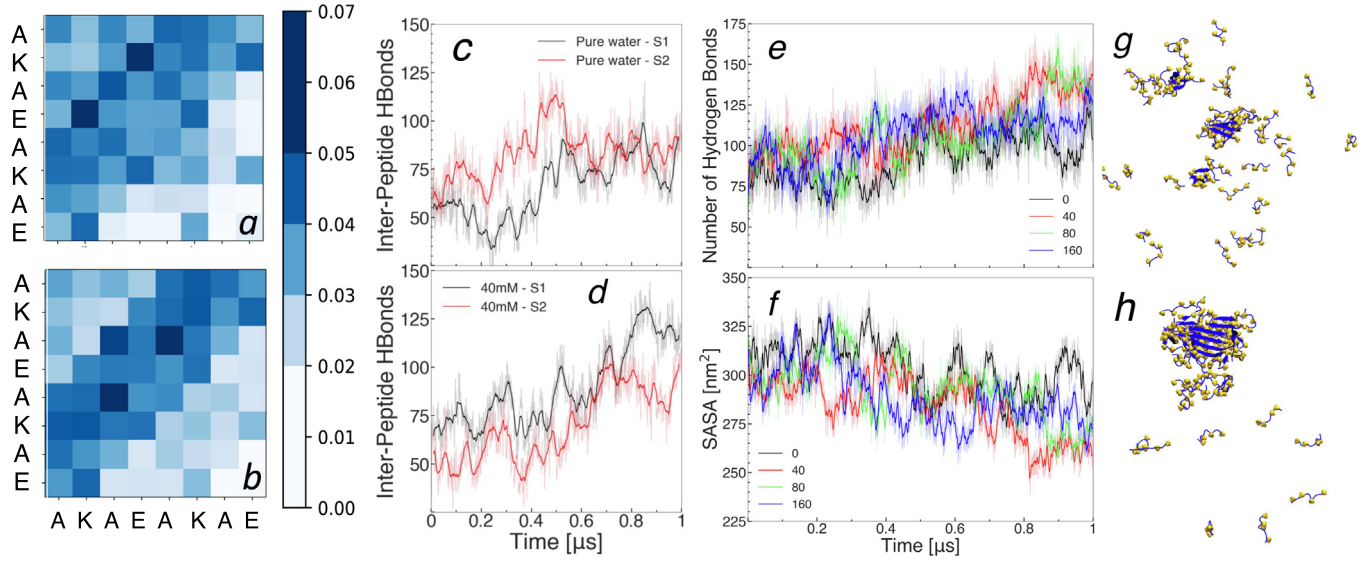


**Fig. 10.** Effects of NaCl on aggregation of A-peptides. Contact maps computed within (a) first and (b) last 500 ns in simulations performed in pure water. Number of inter-hydrogen bonds for two trajectories ($S_1$ and $S_2$) computed in (c) pure water and (d) 40 mM NaCl. (e) Number of hydrogen bonds and (f) SASA in simulations performed in different NaCl concentrations. Final conformations of peptides in simulations performed in (e) pure water, and (f) 40 mM NaCl. For pure water and 40 mM simulations, only trajectory S1 is used in panels a-b and e-h.

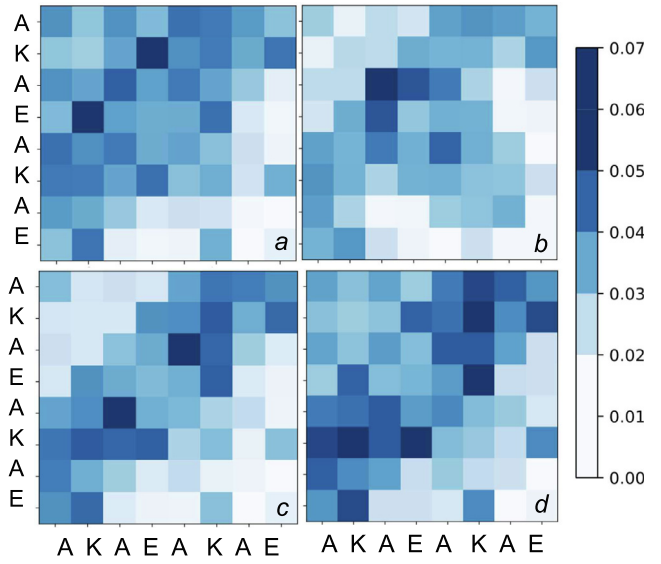


**Fig. 11.** Contact maps computed within the first 500 ns of simulations performed using the A-peptide in (a) pure water, (b) 40 mM, (c) 80 mM, and (d) 160 mM NaCl.

In Fig. 11, we show contact maps computed for the first 500 ns in simulations performed in pure water, 40, 80, and 160 mM of NaCl. The probability of forming contacts between charged residues is high under conditions in which A-peptides do not form a large number of inter-$N_{HB}$, i.e., pure water and solution containing 160 mM NaCl. In contrast, contacts between charged residues are significantly reduced in 40 and 80 mM NaCl solutions where A-peptides form $\beta$-sheet aggregates. This is consistent with our hypothesis that electrostatic contacts between side chains contribute to deter the formation of aggregates for A-peptides. Our results are aligned with a previous study on the AEAKAEAKAEAKAE peptide, also known as EAK16-I. In this study, the addition of NaCl to the solution at concentrations below 20 mM was shown to promote the self-assembly process into fibrils [33]. Notice that an alternative explanation for the effect of salts on aggregation is salting-out wherein the reduced solubility of the A-peptide can be explained by the preference of NaCl to be exposed to the solvent [60].

## 4. Discussion and Conclusion

In summary, we performed extensive all-atom simulations of strictly amphipathic sequences to study their aggregation into amyloid fibrils. We found that this self-assembly process occurs faster with increasing temperature and the formation of fibrils does not take place if non-polar residues are weakly hydrophobic. This latter result is consistent with experimental studies and points to the important role played by hydrophobic interactions in fibril formation [20,22]. Moreover, the faster formation of amyloid fibrils with increasing temperature in our simulations can be attributed to the strength of hydrophobic interactions, which increases with increasing temperature [48–50]. Another important interaction contributing to fibril formation is hydrogen bonding between backbone atoms. As expected, the formation of $\beta$-sheets leads to an increase in the number of backbone hydrogen bonds in our simulations. However, if hydrogen bonds were the main (or only) interaction driving fibril formation, all sequences studied here would form fibril as they have identical backbone atoms and, thus, the same potential to form hydrogen bonds [52]. This is consistent with other computational studies wherein the formation of one peptide-peptide hydrogen bonds was shown to be compensated by the rupture of two peptide-water hydrogen bonds and the formation of one water-water hydrogen bond [61,62]. Also, hydrogen bonds become unstable with increasing temperature [49,50], which cannot explain the temperature dependent rate of fibril formation in our simulations.

We also found a preference of the peptides studied for the formation of anti-parallel $\beta$-sheets. Electrostatic interactions between charged side chains may be responsible for this preference as they can discriminate between parallel and anti-parallel $\beta$-sheets. However, in simulations where the non-polar residue is only weakly hydrophobic, i.e., the A-peptide, electrostatic interactions did not contribute favorably to aggregation: screening these interactions by adding salt to the solution produced a modest increase in aggregation. This is consistent with experimental studies on the AEAKAEAKAEAKAE peptide wherein the addition of NaCl to the solution at concentrations below 20 mM was shown to promote fibril formation [33]. In the same vein, in a recent all-atom simulation study of the A$\beta$ protein, the addition of salt to the solution was shown to screen interactions between charged residues in the middle of the protein [53]. This was shown to destabilize the formation of a $\beta$-sheet between the central-hydrophobic-core and the central-hydrophilic-core of this protein enabling the formation of the turn region observed in some A$\beta$ fibril structures. This could explain the increased rate of fibril formation of this peptide in the presence of salts [63–65].

Fibril growth in our simulations proceeded through the displacement of peptides located in the vicinity of the fibril to the tip. Most peptides were extended, e.g., formed a $\beta$-strand, when deposited on the fibril tip. This is consistent with another computational study on the aggregation of KFFE peptides in which the formation of $\beta$-sheets was suggested to occur in an orderly manner from the beginning to the end of the simulation [30]. However, we also observed the deposition of a peptide that was folded into a $\beta$-hairpin. Within 1 $\mu$s, this hairpin unfolded to adopt a conformation consistent with the fibril template, i.e., a $\beta$-strand. Thus, fibril growth may also take place in a more disordered manner given enough time for conformational defects to relax.

As suggested in previous studies, the sequence pattern determines both the propensity of a peptide to form $\beta$-strands as well as its ability to segregate non-polar and charged residues into difference faces of the $\beta$-sheet [17]. These two properties of a sequence are prerequisites for the formation of fibrils while the net hydrophobicity is required to stabilize packing of $\beta$-sheets into cross-$\beta$ structures [66,21,22,20]. Here, we also performed simulations using KE**FFFFF**KE and (K**FF**E)$_2$ sequences which are made of the same amino acids as the F-peptide but have different propensity to form $\beta$-structures as well as segregate non-polar and charged residues to different faces of a $\beta$-sheet. The propensity of these sequences to form $\beta$-structures and inter-peptide hydrogen bonds in our simulations correlate with their experimental tendency to form cross-$\beta$ structures, i.e., F-peptide > KE**FFFFF**KE > (K**FF**E)$_2$. This suggests that all-atom simulations could become a powerful method to predict a sequence's propensity to form amyloid fibrils, at least for amphipathic sequences. However, simulations have to be performed for much longer (2–3 $\mu$s) than most current all-atom studies (0.5–1 $\mu$s) to be able to differentiate between the aggregation propensity of (K**FF**E)$_2$ and KE**FFFFF**KE peptides–see Fig. 8. Note that bioinformatics tools to predict the propensity of peptides to form amyloid fibrils are not always reliable for designed sequences [67,68]. For example, the order of aggregation predicted using *AGGRESCAN* [69] and *Tango* [70] are KE**FFFFF**KE > F-peptide = (K**FF**E)$_2$ and (K**FF**E)$_2$ > KE**FFFFF**KE > F-peptide, respectively. The latter predicts the reverse order of aggregation compared to experiments, and AGGRESCAN predicts the same aggregation propensity for (K**FF**E)$_2$, which does not form fibrils in experiments, and the F-peptide that is highly aggregation prone.

Despite the important insights brought up by this study, its limitations should also be highlighted. In this work, high temperatures are used in order to observe aggregation in a reasonable timescale. In addition to affecting the balance of the different types of interactions, e.g., increasing the strength of hydrophobic interaction, these high temperature also reduce the viscosity of the system while increasing the overall dynamics of the system. This reduced viscosity and increased dynamics can also contribute to a faster aggregation rate although the opposite is observed for the A-peptide, which formed less inter-peptide hydrogen bonds at higher temperatures. In addition, we found that NaCl has a small tendency to favor aggregation of the less hydrophobic A-peptide. Our simulations are however subjected to large fluctuations and more extensive simulations are needed to provide insights into how this tendency is affected by the concentration of NaCl. At last, due to the large computational cost of performing the simulations in this work, some of our results were obtained from analysis of a single trajectory. This includes a proposed mechanism in which peptides are displaced from the vicinity of a fibril to its tip to account for its growth.

## Declaration of Competing Interest

The authors declare that they have no known competing financial interests or personal relationships that could have appeared to influence the work reported in this paper.

## Acknowledgement

This work supported by the National Science Foundation under Grant Nos. CHE-1904364 and CHE-1904528. Computational resources were provided by Academic and Research Computing Systems (ARCS) at the New Jersey Institute of Technology and by the Pittsburgh Supercomputing Center (PSC). Anton 2 at PSC is supported by the National Institute of General Medical Sciences of the National Institute of Health under Award Number R01GM116961. The Anton 2 machine at PSC was generously made available by D.E. Shaw Research.

## Appendix A. Supplementary material

Supplementary data associated with this article can be found, in the online version, at https://doi.org/10.1016/j.molliq.2021.118283.

## References

[1] Fabrizio Chiti, Christopher M. Dobson, Protein misfolding, functional amyloid, and human disease, Annu. Rev. Biochem. 75 (2006) 333–366.
[2] Fabrizio Chiti, Christopher M. Dobson, Protein misfolding, amyloid formation, and human disease: a summary of progress over the last decade, Annual review of biochemistry 86 (2017) 27–68.
[3] Ximena Zottig, Mélanie Côté-Cyr, Dominic Arpin, Denis Archambault, Steve Bourgault, Protein supramolecular structures: From self-assembly to nanovaccine design, Nanomaterials 10 (5) (2020) 1008.
[4] Aaron M. Kushner, Zhibin Guan, Modular design in natural and biomimetic soft materials, Angew. Chem. Int. Ed. 50 (39) (2011) 9026–9057.
[5] Charlotte J.C. Edwards-Gayle, Ian W. Hamley, Self-assembly of bioactive peptides, peptide conjugates, and peptide mimetic materials, Organic & biomolecular chemistry 15 (28) (2017) 5867–5876.
[6] Ashkan Dehsorkhi, Valeria Castelletto, Ian W. Hamley, Self-assembling amphiphilic peptides, J. Pept. Sci. 20 (7) (2014) 453–467.
[7] Karen E. Marshall, Devkee M. Vadukul, Liza Dahal, Alina Theisen, Milena W. Fowler, Youssra Al-Hilaly, Lenzie Ford, György Kemenes, Iain J. Day, Kevin Staras, et al., A critical role for the self-assembly of amyloid-$\beta$1-42 in neurodegeneration, Scientific reports 6 (1) (2016) 1–13.
[8] Li Deng, Peng Zhou, Yurong Zhao, Yanting Wang, Xu. Hai, Molecular origin of the self-assembled morphological difference caused by varying the order of charged residues in short peptides, J. Phys. Chem. B 118 (43) (2014) 12501–12510.
[9] George M. Whitesides, Mila Boncheva, Beyond molecules: Self-assembly of mesoscopic and macroscopic components, Proc. Nat. Acad. Sci. 99 (8) (2002) 4769–4774.
[10] Shuguang Zhang, Davide M. Marini, Wonmuk Hwang, Steve Santoso, Design of nanostructured biological materials through self-assembly of peptides and proteins, Current opinion in chemical biology 6 (6) (2002) 865–871.
[11] Rebecca Nelson, Michael R. Sawaya, Melinda Balbirnie, Anders Ø Madsen, Christian Riekel, Robert Grothe, David Eisenberg, Structure of the cross-$\beta$spine of amyloid-like fibrils, Nature 435 (7043) (2005) 773–778.
[12] Tuomas P. Knowles, Anthony W. Fitzpatrick, Sarah Meehan, Helen R. Mott, Michele Vendruscolo, Christopher M. Dobson, Mark E. Welland, Role of intermolecular forces in defining material properties of protein nanofibrils, Science 318 (5858) (2007) 1900–1903.
[13] Birgit Strodel, Amyloid aggregation simulations: challenges, advances and perspectives, Current opinion in structural biology 67 (2021) 145–152.
[14] Martín Carballo-Pacheco, Birgit Strodel, Advances in the simulation of protein aggregation at the atomistic scale, J. Phys. Chem. B 120 (12) (2016) 2991–2999, PMID: 26965454.
[15] Charles J. Bowerman, Bradley L. Nilsson, Review self-assembly of amphipathic $\beta$-sheet peptides: insights and applications, Pept. Sci. 98 (3) (2012) 169–184.
[16] Silvia Cavalli, Fernando Albericio, Alexander Kros, Amphiphilic peptides and their cross-disciplinary role as building blocks for nanoscience, Chem. Soc. Rev. 39 (1) (2010) 241–263.
[17] Naomi R. Lee, Charles J. Bowerman, Bradley L. Nilsson, Effects of varied sequence pattern on the self-assembly of amphipathic peptides, Biomacromolecules 14 (9) (2013) 3267–3277.
[18] Michael R. Sawaya, Shilpa Sambashivan, Rebecca Nelson, Magdalena I. Ivanova, Stuart A. Sievers, Marcin I. Apostol, Michael J. Thompson, Melinda Balbirnie, Jed J.W. Wiltzius, Heather T. McFarlane, et al., Atomic structures of amyloid cross-$\beta$spines reveal varied steric zippers, Nature 447 (7143) (2007) 453–457.
[19] David S. Eisenberg, Michael R. Sawaya, Structural studies of amyloid proteins at the molecular level, Annual review of biochemistry 86 (2017) 69–95.
[20] Charles J. Bowerman, Derek M. Ryan, David A. Nissan, Bradley L. Nilsson, The effect of increasing hydrophobicity on the self-assembly of amphipathic $\beta$-sheet peptides, Mol. BioSyst. 5 (9) (2009) 1058–1069.
[21] Ria J. Betush, Jennifer M. Urban, Bradley L. Nilsson, Balancing hydrophobicity and sequence pattern to influence self-assembly of amphipathic peptides, Pept. Sci. 110 (1) (2018) e23099.
[22] A. Saiani, A. Mohammed, H. Frielinghaus, R. Collins, N. Hodson, C.M. Kielty, M.J. Sherratt, A.F. Miller, Self-assembly and gelation properties of $\alpha$-helix versus $\beta$-sheet forming peptides, Soft Matter 5 (1) (2009) 193–202.
[23] Ioana M. Ilie, Amedeo Caflisch, Simulation studies of amyloidogenic polypeptides and their aggregates, Chemical reviews 119 (12) (2019) 6956–6993.
[24] Giovanni Bellesia, Joan-Emma Shea, Effect of $\beta$-sheet propensity on peptide aggregation, J. Chem. Phys. 130 (14) (2009) 04B610.
[25] Riccardo Pellarin, Amedeo Caflisch, Interpreting the aggregation kinetics of amyloid peptides, Journal of molecular biology 360 (4) (2006) 882–892.
[26] Yiming Wang, Samuel J. Bunce, Sheena E. Radford, Andrew J. Wilson, Stefan Auer, Carol K. Hall, Thermodynamic phase diagram of amyloid-$\beta$(16–22) peptide, Proc. Nat. Acad. Sci. 116 (6) (2019) 2091–2096.
[27] Soheila Emamyari, Faezeh Kargar, Vahid Sheikh-Hasani, Saeed Emadi, Hossein Fazli, Mechanisms of the self-assembly of eak16-family peptides into fibrillar and globular structures: molecular dynamics simulations from nano-to micro-seconds, Eur. Biophys. J. 44 (4) (2015) 263–276.
[28] Suman Samantray, Feng Yin, Batuhan Kav, Birgit Strodel, Different force fields give rise to different amyloid aggregation pathways in molecular dynamics simulations, J. Chem. Inf. Model. 60 (12) (2020) 6462–6475.
[29] Workalemahu M. Berhanu, Ulrich H.E. Hansmann, Side-chain hydrophobicity and the stability of a$\beta$16–22 aggregates, Protein Sci. 21 (12) (2012) 1837–1848.
[30] Ushnish Sengupta, Martín Carballo-Pacheco, Birgit Strodel, Automated markov state models for molecular dynamics simulations of aggregation and self-assembly, The Journal of chemical physics 150 (11) (2019) 115101.
[31] Davide M. Marini, Wonmuk Hwang, Douglas A. Lauffenburger, Shuguang Zhang, Roger D. Kamm, Left-handed helical ribbon intermediates in the self-assembly of a $\beta$-sheet peptide, Nano Lett. 2 (4) (Apr 2002) 295–299.
[32] Wonmuk Hwang, Davide M. Marini, Roger D. Kamm, Shuguang Zhang, Supramolecular structure of helical ribbons self-assembled from a $\beta$-sheet peptide, The Journal of chemical physics 118 (1) (2003) 389–397.
[33] Yooseong Hong, Lue Shunn Lau, Raymond L. Legge, P. Chen, Critical self-assembly concentration of an ionic-complementary peptide eak16-i, The Journal of Adhesion 80 (10–11) (2004) 913–931.
[34] Kresten Lindorff-Larsen, Stefano Piana, Kim Palmo, Paul Maragakis, John L. Klepeis, Ron O. Dror, David E. Shaw, Improved side-chain torsion potentials for the amber ff99sb protein force field, Proteins: Struct., Funct., Bioinf. 78 (8) (2010) 1950–1958.
[35] Michael P. Allen, Dominic J. Tildesley, Computer simulation of liquids, Oxford University Press, 2017.
[36] Michele Parrinello, Aneesur Rahman, Polymorphic transitions in single crystals: A new molecular dynamics method, Journal of Applied physics 52 (12) (1981) 7182–7190.
[37] Par Bjelkmar, Per Larsson, Michel A. Cuendet, Berk Hess, Erik Lindahl, Implementation of the charmm force field in gromacs: analysis of protein

stability effects from correction maps, virtual interaction sites, and water models, Journal of chemical theory and computation 6 (2) (2010) 459–466.
[38] Mark James Abraham, Teemu Murtola, Roland Schulz, Szilárd Páll, Jeremy C. Smith, Berk Hess, Erik Lindahl, Gromacs: High performance molecular simulations through multi-level parallelism from laptops to supercomputers, SoftwareX 1 (2015) 19–25.
[39] David E. Shaw, J.P. Grossman, Joseph A. Bank, Brannon Batson, J. Adam Butts, Jack C. Chao, Martin M. Deneroff, Ron O. Dror, Amos Even, Christopher H. Fenton, et al. Anton 2: raising the bar for performance and programmability in a special-purpose molecular dynamics supercomputer, in: SC'14: Proceedings of the International Conference for High Performance Computing, Networking, Storage and Analysis, pages 41–53. IEEE, 2014.
[40] Supplemental information.
[41] Xuzhi Hu, Mingrui Liao, Haoning Gong, Lin Zhang, Henry Cox, Thomas A. Waigh, Jian R. Lu, Recent advances in short peptide self-assembly: from rational design to novel applications, Current Opinion in Colloid & Interface Science 45 (2020) 1–13.
[42] Suman Samantray, Wibke Schumann, Alexander-Maurice Illig, Martin Carballo-Pacheco, Arghadwip Paul, Bogdan Barz, and Birgit Strodel. Molecular dynamics simulations of protein aggregation: protocols for simulation setup and analysis with markov state models and transition networks. bioRxiv, 2020.
[43] Richard J. Gowers, Max Linke, Jonathan Barnoud, Tyler John Edward Reddy, Manuel N. Melo, Sean L. Seyler, Jan Domanski, David L Dotson, Sébastien Buchoux, Ian M Kenney, et al. Mdanalysis: a python package for the rapid analysis of molecular dynamics simulations. Technical report, Los Alamos National Lab. (LANL), Los Alamos, NM (United States), 2019.
[44] Naveen Michaud-Agrawal, Elizabeth J. Denning, Thomas B. Woolf, Oliver Beckstein, Mdanalysis: a toolkit for the analysis of molecular dynamics simulations, Journal of computational chemistry 32 (10) (2011) 2319–2327.
[45] Robert T. McGibbon, Kyle A. Beauchamp, Matthew P. Harrigan, Christoph Klein, Jason M. Swails, Carlos X. Hernández, Christian R. Schwantes, Lee-Ping Wang, Thomas J. Lane, Vijay S. Pande, Mdtraj: a modern open library for the analysis of molecular dynamics trajectories, Biophysical journal 109 (8) (2015) 1528–1532.
[46] Wolfgang Kabsch, Christian Sander, Dictionary of protein secondary structure: pattern recognition of hydrogen-bonded and geometrical features, Biopolymers: Original Research on Biomolecules 22 (12) (1983) 2577–2637.
[47] Meiwen Cao, Yu. Yang Shen, Xiaoling Wang Wang, Dongxiang Li, Self-assembly of short elastin-like amphiphilic peptides: Effects of temperature, molecular hydrophobicity and charge distribution, Molecules 24 (1) (2019) 202.
[48] Walter Kauzmann, Some factors in the interpretation of protein denaturation, Advances in protein chemistry 14 (1959) 1–63.
[49] Ken A Dill, Dominant forces in protein folding, Biochemistry 29 (31) (1990) 7133–7155.
[50] Cristiano L Dias, Teemu Hynninen, Tapio Ala-Nissila, Adam S Foster, Mikko Karttunen, Hydrophobicity within the three-dimensional mercedes-benz model: Potential of mean force, The Journal of chemical physics 134 (6) (2011) 02B620.
[51] Cristiano L Dias, Tapio Ala-Nissila, Jirasak Wong-ekkabut, Ilpo Vattulainen, Martin Grant, Mikko Karttunen, The hydrophobic effect and its role in cold denaturation, Cryobiology 60 (1) (2010) 91–99.
[52] Su. Zhaoqian, Cristiano L Dias, Driving $\beta$-strands into fibrils, J. Phys. Chem. B 118 (37) (2014) 10830–10836.
[53] Farbod Mahmoudinobar, Bradley L Nilsson, Cristiano L Dias, Effects of ions and small compounds on the structure of a$\beta$42 monomers, J. Phys. Chem. B 125 (4) (2021) 1085–1097.
[54] Rajesh Mishra, Roland Winter, Cold-and pressure-induced dissociation of protein aggregates and amyloid fibrils, Angew. Chem. Int. Ed. 47 (35) (2008) 6518–6521.
[55] Lena Ostermeier, Guilherme AP de Oliveira, Wojciech Dzwolak, Jerson L Silva, Roland Winter, Exploring the polymorphism, conformational dynamics and function of amyloidogenic peptides and proteins by temperature and pressure modulation, Biophys. Chem. 268 (2021) 106506.
[56] J.H.M. an Gils, E. van Dijk, A. Peduzzo, A. Hofmann, N. Vettore, M.P. Schützmann, G. Groth, H. Mouhib, D.E. Otzen, A.K. Buell, and S. Abeln. The hydrophobic effect characterises the thermodynamic signature of amyloid fibril growth. PLOS Comp. Biol., 16:e1007767, 2020.
[57] Susan Costantini, Giovanni Colonna, Angelo M Facchiano, Amino acid propensities for secondary structures are influenced by the protein structural class, Biochemical and biophysical research communications 342 (2) (2006) 441–451.
[58] Stefan Tsonchev, Krista L Niece, George C Schatz, Mark A Ratner, Samuel I Stupp, Phase diagram for assembly of biologically-active peptide amphiphiles, J. Phys. Chem. B 112 (2) (2008) 441–447.
[59] Yooseong Hong, Raymond L Legge, S. Zhang, P. Chen, Effect of amino acid sequence and ph on nanofiber formation of self-assembling peptides eak16-ii and eak16-iv, Biomacromolecules 4 (5) (2003) 1433–1442.
[60] Ronen Zangi, Can salting-in/salting-out ions be classified as chaotropes/kosmotropes?, J Phys. Chem. B 114 (1) (2010) 643–650.
[61] Chitra Narayanan and Cristiano L Dias. Hydrophobic interactions and hydrogen bonds in $\beta$-sheet formation. The journal of chemical physics, 139 (11):09B640_1, 2013.
[62] William L Jorgensen, Interactions between amides in solution and the thermodynamics of weak binding, J. Am. Chem. Soc. 111 (10) (1989) 3770–3771.
[63] Axel Abelein, Jüri Jarvet, Andreas Barth, Astrid Gräslund, Jens Danielsson, Ionic strength modulation of the free energy landscape of a$\beta$40 peptide fibril formation, J. Am. Chem. Soc. 138 (21) (2016) 6893–6902.
[64] Aditi Sharma, Sven H Behrens, Yury O Chernoff, Andreas S Bommarius, Modulation of the formation of a$\beta$-and sup35nm-based amyloids by complex interplay of specific and nonspecific ion effects, J. Phys. Chem. B 122 (19) (2018) 4972–4981.
[65] Karolin Klement, Karin Wieligmann, Jessica Meinhardt, Peter Hortschansky, Walter Richter, Marcus Fändrich, Effect of different salt ions on the propensity of aggregation and on the structure of alzheimer's a$\beta$(1–40) amyloid fibrils, Journal of molecular biology 373 (5) (2007) 1321–1333.
[66] Farbod Mahmoudinobar, Jennifer M Urban, Su. Zhaoqian, Bradley L Nilsson, Cristiano L Dias, Thermodynamic stability of polar and nonpolar amyloid fibrils, Journal of chemical theory and computation 15 (6) (2019) 3868–3874.
[67] Bartholomew P Roland, Ravindra Kodali, Rakesh Mishra, Ronald Wetzel, A serendipitous survey of prediction algorithms for amyloidogenicity, Pept. Sci. 100 (6) (2013) 780–789.
[68] Thanh D Do, Nicholas J Economou, Nichole E LaPointe, William M Kincannon, Christian Bleiholder, Stuart C Feinstein, David B Teplow, Steven K Buratto, Michael T Bowers, Factors that drive peptide assembly and fibril formation: experimental and theoretical analysis of sup35 nnqqny mutants, J. Phys. Chem. B 117 (28) (2013) 8436–8446.
[69] Oscar Conchillo-Solé, Natalia S de Groot, Francesc X Avilés, Josep Vendrell, Xavier Daura, Salvador Ventura, Aggrescan: a server for the prediction and evaluation of hot spots of aggregation in polypeptides, BMC bioinformatics 8 (1) (2007) 1–17.
[70] Ana-Maria Fernandez-Escamilla, Frederic Rousseau, Joost Schymkowitz, Luis Serrano, Prediction of sequence-dependent and mutational effects on the aggregation of peptides and proteins, Nature biotechnology 22 (10) (2004) 1302–1306.